5th International Conference on Computational and Mathematical Biomedical Engineering – CMBE2017
10-12 April 2017, United States
P. Nithiarasu, A.M. Robertson (Eds.)

# INVESTIGATING DEMENTIA VIA A MULTICOMPARTMENTAL POROELASTIC MODEL OF PARENCHYMAL TISSUE

**Liwei Guo[1], John C. Vardakis[1], Toni Lassila[3], Dean Chou[2], Brett J. Tully[3], Nishant Ravikumar[7], Micaela Mitolo[5], Matthias Lange[4], Ali Sarrami[4], Zeike A. Taylor[7], Susheel Varma[5], Annalena Venneri[4,5] & Alejandro F. Frangi[4] & Yiannis Ventikos[1]**

[1] Department of Mechanical Engineering, University College London, UK, {liwei.guo, y.ventikos}@ucl.ac.uk
[2] Institute of Biomedical Engineering & Department of Engineering Science, University of Oxford, UK
[3] First Light Fusion Ltd, Begbroke Science Park, Oxfordshire, UK
[4] Centre for Computational Imaging & Simulation Technologies in Biomedicine (CISTIB), Department of Electronic and Electrical Engineering, University of Sheffield, UK
[5] IRCCS San Camillo Foundation Hospital, Venice, Italy
[6] Department of Neuroscience, Medical School, University of Sheffield, UK
[7] Centre for Computational Imaging & Simulation Technologies in Biomedicine (CISTIB), Department of Mechanical Engineering, University of Sheffield, UK

## SUMMARY

In this paper, a workflow within the VPH-DARE@IT Clinical Research Platform is presented. This is used to model the biomechanical behaviour of perfused brain tissue. This workflow features a 3D multicompartmental poroelastic framework, patient-specific brain anatomy representations and continuous waveforms of internal carotid and vertebral arteries, which are used as a means of personalizing the boundary conditions that feed the arterial compartment of the in-house poroelastic solver. Results are shown comparing CSF/ISF clearance and accumulation in two males of similar age, both are non-smokers, however one is more active and is diagnosed with MCI and experiences less sleep.

**Key words:** *Dementia, Poroelasticity, Periventricular Lucency, FEM*

## 1 INTRODUCTION

Dementia is a general term for a range of progressive, organic brain diseases that are characterized by problems of short-term memory, disturbances in language, psychological changes, psychiatric changes and lifestyle impairments [1-3].

Forty-six million people currently live with dementia [4], whilst by 2050, this number is expected to rise to 132 million [5]. The estimated cost of Dementia will increase from $818 billion in 2015 to over $1,000 billion by 2018 [5].

Mild cognitive impairment (MCI) is defined as a state between normal aging and dementia. It is defined as objective cognitive impairment relative to the person's age, with concern about the cognitive symptoms, in a person with essentially normal functional activities who does not have dementia [6]. It affects 19% of people age 65 and over [7]. Around 46% of people with MCI develop dementia within 3 years, compared with 3% of the age-matched population [8].

The capability to model transport of the fluid content of the brain, in a personalised manner and from first principles, is essential for enhancing the biomechanical understanding of functional features like perfusion and clearance. This understanding is expected to yield novel information (and novel biomarkers) especially regarding early stages of diseases of old age, such as dementia.

In this paper, we describe a consolidated pipeline which embeds the following: (i) the three dimensional finite element based discretization of the multiple-network poroelastic theory (MPET), (ii) MRI image acquisition, segmentation, surface correction, smoothing and ultimately mesh generation of the parenchymal and cerebroventricular volumes and finally, (iii) a subject-specific boundary condition model consisting of a coupled lumped parameter circulation model, surrogate model and cerebral autoregulation model.

## 2 METHODOLOGY

### *2.1 Multiple-Network Poroelastic Theory (MPET)*

MPET is used to develop a spatio-temporal model of tissue displacement and fluid regulation in varying scales within the cerebral environment. The field equations are discretized using the finite-element method, and in all three spatial dimensions.

Specifically, the field equations of the MPET system stem from the fully dynamic, classical Biot system [9]. For a single compartment, this consists of the Navier equation representing momentum balance, and the Duhamel equation for the mass balance representing the diffusive Darcy fluid flow:

$$\begin{aligned} &\rho\ddot{\mathbf{u}} - (\lambda+\mu)\nabla(\nabla\cdot\mathbf{u}) - \mu\nabla^2\mathbf{u} + \alpha\nabla p = \mathbf{f} \\ &\gamma\dot{p} + \alpha\nabla\cdot\dot{\mathbf{u}} - \nabla\cdot\boldsymbol{\kappa}(\nabla p - \rho_f\mathbf{g}) = s \end{aligned} \tag{1a, b}$$

In equations 1a and 1b, $\rho$ represents the density of a porous and permeable matrix, $\rho_f$ represents the density of the fluid, λ and μ are the Lamé parameters (dilation and shear moduli of elasticity), α is the Biot-Willis constant, $\boldsymbol{\kappa}$ is the symmetric permeability tensor divided by the fluid viscosity, γ is the constrained specific storage coefficient, **g** is the gravity vector, *s* is a source/sink term and finally, **u** and *p* are the solid matrix displacement (mean displacement of particles forming the solid matrix) and the scalar pore pressure, respectively.

In its current form, the MPET model comprises of four separate fluid compartments, arterial blood (a), arteriole/capillary blood (c), venous blood (v) and CSF/ISF (e) [9]. The resulting MPET system is:

$$\begin{aligned} &G\nabla^2\boldsymbol{u} + (G+\lambda)\nabla(\nabla\cdot\boldsymbol{u}) = (\alpha_a\nabla p_a + \alpha_c\nabla p_c + \alpha_e\nabla p_e + \alpha_v\nabla p_v) - \boldsymbol{F} \\ &\gamma_a\frac{\partial p_a}{\partial t} + \alpha_a\frac{\partial}{\partial t}(\nabla\cdot\boldsymbol{u}) = \boldsymbol{\kappa}_a\nabla^2 p_a + (s_{c\to a} + s_{e\to a} + s_{v\to a}) \\ &\gamma_c\frac{\partial p_c}{\partial t} + \alpha_c\frac{\partial}{\partial t}(\nabla\cdot\boldsymbol{u}) = \boldsymbol{\kappa}_c\nabla^2 p_c + (s_{a\to c} + s_{e\to c} + s_{v\to c}) \\ &\gamma_e\frac{\partial p_e}{\partial t} + \alpha_e\frac{\partial}{\partial t}(\nabla\cdot\boldsymbol{u}) = \boldsymbol{\kappa}_e\nabla^2 p_e + (s_{a\to e} + s_{c\to e} + s_{v\to e}) \\ &\gamma_v\frac{\partial p_v}{\partial t} + \alpha_v\frac{\partial}{\partial t}(\nabla\cdot\boldsymbol{u}) = \boldsymbol{\kappa}_v\nabla^2 p_v + (s_{a\to v} + s_{c\to v} + s_{e\to v}) \end{aligned} \tag{2a-e}$$

In the above equations, the fluid phase continuity equations include the sum of all interporosity fluxes ($s_{xy}$), from network *y* to *x*. Here, the transfer is considered to be driven by a hydrostatic pressure gradient (of the form, $s_{xy} = \omega_{xy}(p_y - p_x)$), where $\omega_{xy}$ is the transfer coefficient scaling the flow from network *y* to network *x*.

### *2.2 Verification of MPET poroelastic solver*

In order to ascertain the accuracy of the 3D MPET poroelastic solver, the numerical code is verified against two consolidation problems, i.e. Terzaghi's and Mandel's [10,11] problems, respectively. In both of these simulations, a special case of the MPET system is utilized, specifically that of using a single compartment. Excellent agreement exists between the analytical and numerical solutions.

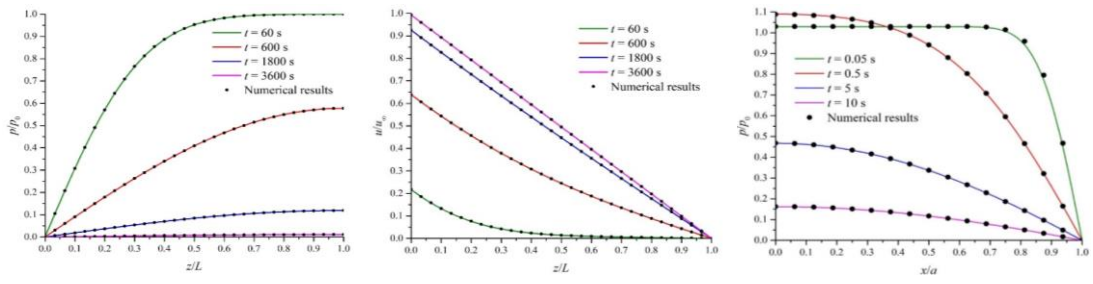


**Figure 1.** *Terzaghi's 1D consolidation problem*: (Left) Plots of dimensionless pore pressure against dimensionless vertical distance. (Center) Plots of dimensionless vertical displacement against dimensionless vertical distance. *Mandel's 2D consolidation problem*: (Right) Plots of dimensionless pore pressure against dimensionless horizontal distance from the center. Coloured curves represent the analytical solutions in all three plots.

*2.3 Consolidated pipeline*

A depiction of the consolidated pipeline can be seen in Figure 2 below. The personalization of the cerebral geometries is achieved by a separate pipeline that comprises of: (i) Image segmentation of sub-cortical and whole brain segmentation of T1-weighted images, (ii) Diffusion tensor field estimation, (iii) Image registration, (iv) volumetric mesh generation and (v) permeability tensor field interpolation.

The second integral component of the consolidate pipeline involves an overarching subject-specific boundary condition model, intricately consisting of a lumped parameter circulation model, surrogate model and cerebral autoregulation model. This component yields subject specific boundary condition profiles for the arterial compartment of the MPET system, and is able to provide subject-specific measurements of internal carotid and vertebral artery flow in both left and right sides of the cerebrum and cerebellum. These values are divided by the surface area of each corresponding surface region (left/right cerebellum/cerebrum) and subsequently converted into a Neumann boundary condition via the use of the porosity of the arterial compartment. This ultimately gives rise to a detailed atlas of voxel specific arterial pore pressures, which have been directly influenced by the adoption of the feeding territories as boundary conditions.

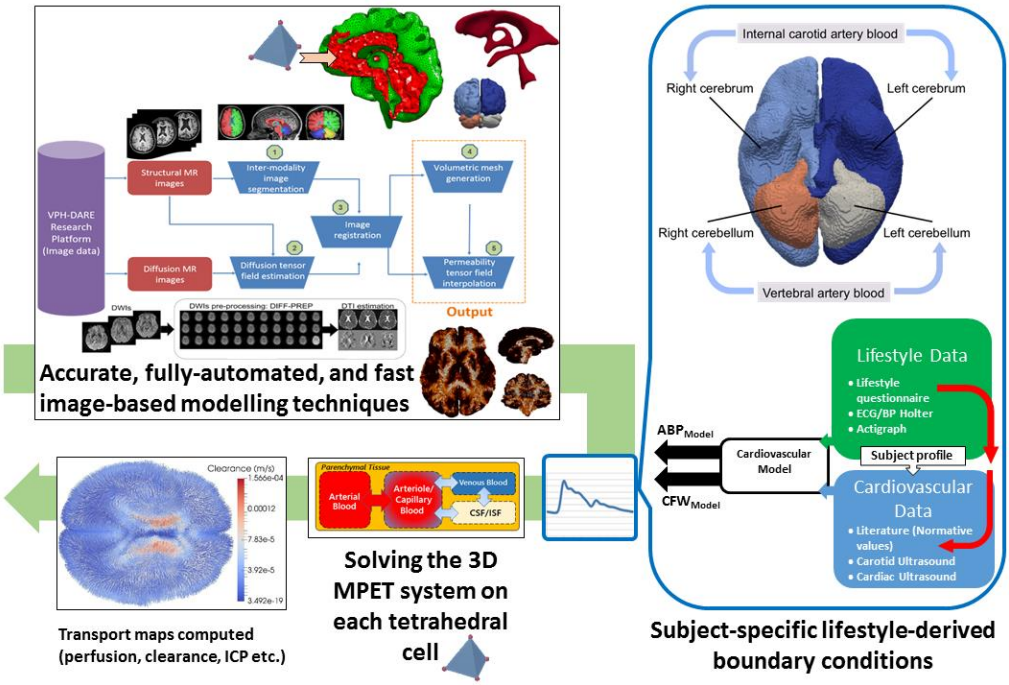


**Figure 2.** Consolidated poroelastic pipeline.

## 3 RESULTS AND CONCLUSIONS

In Figure 3 below, a sample of the type of results that can be investigated in detail are shown. The below results correspond to a period of high activity for both MCI patient and control subject. In this set of results, Control 18 corresponds to a 77-year-old male, non-smoker, weighing 64 kg and has stated that he spends between 15-29 minutes per day on leisure activities and an average sleeping pattern. MCI 16 is a 78-year-old male with MCI, a non-smoker, weighing 70 kg, spends over 1 hour on his daily leisure whilst only achieving just under 6 hours of sleep. The CSF/ISF clearance corresponds to the Darcy filtration velocity of the CSF/ISF compartment, whilst CSF/ISF accumulation corresponds to the fluid increment in the same compartment. Periventricularly, it can be seen in Figure 3 that clearance of CSF/ISF is high, with the MCI patient exhibiting a lower peak CSF/ISF clearance of ~ 0.8 μm/s compared to ~ 5 μm/s for the control subject in the deep parenchyma. Both control and MCI cases appear to have a similar peak clearance rate of ~ 1 cm/s.

For the results allied to CSF/ISF accumulation, it is observed that fluid tends to accumulate around the ventricles yet also exhibits peak drainage at the ventricular areas of highest concavity. The MCI patient accumulates and drains more CSF/ISF compared to the healthy case, even though the ventricular volume is smaller for the MCI patient. This qualitatively agrees with previous results [9]. Periventricular lucency (PVL) [12] is represented by increased CSF/ISF content in the

periventricular regions, and is stipulated to be a result of ependymal surface breakdown. In theory, this helps alleviate some of the increased pressure in the ventricles by allowing for some CSF extravasation and subsequently edema formation (frontal horns, where peak drainage occurs). This mechanism could be achieved with the possible assistance of Aquaporin-4 [13], which lines the ependymal surface. Peña and colleagues [14] describe how the concavity of the ventricles helps accumulate expansive stresses on the horns of the ventricles, which as is now known could induce swelling activated $Cl^-$ channels such in microglia, and therefore facilitate periventricular lucency [15,16].

Results corresponding to a period of low activity (sleep) for the same subject and patient show a CSF/ISF clearance (range of ~ 1cm/s to ~ 5 μm/s) and fluid accumulation (2.35 to -0.2) for the healthy case, and a range of ~ 7 mm/s to ~ 0.3 μm/s and 2.66 to -1.15 for the MCI patient respectively. This type of comparison may assist in the interrogation of whether a paravascular pathway facilitates the clearance of solutes from the brain parenchyma, as it has been shown that mice lacking astrocytic Aquaporin-4 exhibit reduced solute clearance (such as amyloid-β). This type of modelling could therefore aid in providing valuable information allied to disease progression in Alzheimer's disease [17]. Other sets of results currently being scrutinized include a healthy 82-year-old female and an 83-year-old female with MCI and two 66-year-old males (control and MCI).

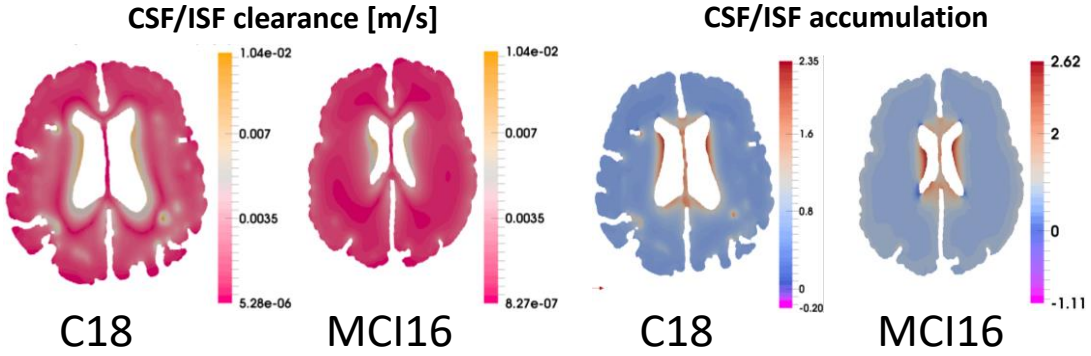


**Figure 3**. CSF/ISF clearance (left pair) and CSF/ISF accumulation (right pair) results for the control (C18) and MCI (MCI16) case respectively.

## REFERENCES


[1] L. Di Marco et al., Modifiable Lifestyle Factors in Dementia: A Systematic Review of Longitudinal Observational Cohort Studies. Journal of Alzheimer's Disease, 42, 2014.

[2] SM. Orton et al., Sex ratio of multiple sclerosis in Canada: a longitudinal study. Lancet Neurol. 5, 2006.

[3] CC. Whitacre et al., A Gender Gap in Autoimmunity: Task Force on Gender, Multiple Sclerosis and Autoimmunity. Science, 283, 1999.

[4] WT. Mayr et al., Incidence and prevalence of multiple sclerosis in Olmsted County, Minnesota, 1985-2000. Neurology, 61, 2003.

[5] M. Prince et al., International AsD. World Alzheimer Report (Journey of Caring. An analysis of long-term care for dementia.). Alzheimer's Disease International (ADI), 2015.

[6] C. Cooper et al., Modifiable Predictors of Dementia in Mild Cognitive Impairment: A Systematic Review and Meta-Analysis. American Journal of Psychiatry, 172:4, 2015.

[7] OL. Lopez et al., Incidence of dementia in mild cognitive impairment in the Cardiovascular Health Study Cognition Study. Arch Neurol, 64, 2007.

[8] JT. Tschanz et al., Cache County Investigators: Conversion to dementia from mild cognitive disorder: the Cache County Study. Neurology, 67, 2006.

[9] JC. Vardakis et al. Investigating cerebral oedema using poroelasticity. Medical Engineering & Physics, 38:1, 2016.

[10] K. Terzaghi, Erdbaumechanik auf Bodenphysikalischer Grundlage. Vienna, F. Duticke, 1925

[11] J. Mandel, Géotechnique, 3:7, 1953.

[12] TP. Naidich et al. Evaluation of Pediatric Hydrocephalus by Computed Tomography. Radiology, 119:2, 1976.

[13] MC. Papadopoulos, AS. Verkman. Aquaporin water channels in the nervous system. Nat Rev Neurosci, 14:4, 2013.

[14] A. Peña, et al. Effects of brain ventricular shape on periventricular biomechanics: a finite-element analysis. Neurosurgery, 45:1, 1999.

[15] A. Fukuda, J. Badaut. Aquaporin 4: a player in cerebral edema and neuroinflammation. J Neuroinflamm, 9:1, 2012.

[16] L.C. Schlichter, T. Mertens, B. Liu. Swelling activated Cl- channels in microglia: biophysics, pharmacology and role in glutamate release. Channels (Austin), 5:2, 2011.

[17] JJ. Iliff et al. A Paravascular Pathway Facilitates CSF Flow Through the Brain Parenchyma and the Clearance of Interstitial Solutes, Including Amyloid. Science Translational Medicine, 4:147, 2012.